THE JOURNAL OF PHYSICAL CHEMISTRY LETTERS
A JOURNAL OF THE AMERICAN CHEMICAL SOCIETY

pubs.acs.org/JPCL

Letter

Pump-Intensity Scaling of Two-Photon Absorption and Photon Statistics of Entangled-Photon Fields

Deependra Jadoun, Upendra Harbola, Vladimir Y. Chernyak, and Shaul Mukamel*

Cite This: J. Phys. Chem. Lett. 2025, 16, 4547−4554

Read Online

ACCESS | Metrics & More | Article Recommendations | Supporting Information

ABSTRACT: We use a nonperturbative theoretical approach to the parametric down-conversion (PDC) process, which generates an entangled-photon field for an arbitrarily strong pump-pulse. This approach can be used to evaluate multipoint field correlation functions to compute nonlinear spectroscopic signals induced by a strong pump. The entangled-photon statistics is studied using Glauber's $g^{(2)}$ function, which helps understand the significance of the photon entanglement-time and the pump-pulse intensity on spectroscopic signals. Under the nonperturbative treatment of the entangled field, the two-photon absorption (TPA) signal shows linear to strongly nonlinear growth with the pump intensity, rather than the linear to quadratic scaling reported previously. An increase in the range of pump intensity for the linear scaling is observed as the pump bandwidth is increased. We propose an experimental scheme that can select contributions to the TPA signal that arise solely from interactions with the entangled photons, and filter out unentangled-photon contributions, which are dominant at higher pump intensities, paving a way to explore the entanglement effects at higher intensities.

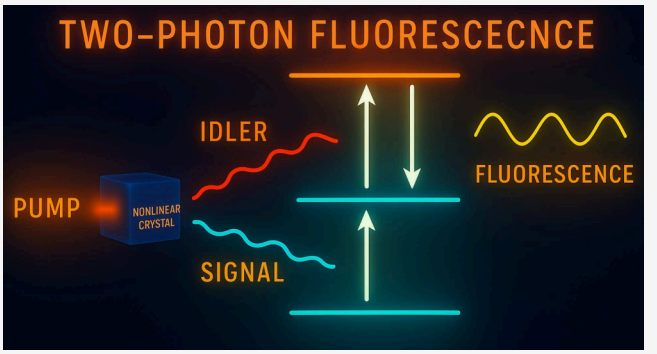

Entanglement is a quantum mechanical effect that correlates two or more particles in a nonclassical way. An entangled pair of photons, also known as quantum light, is one such example where the time-energy entanglement between the two entangled photons can be utilized in spectroscopy to gain insights into the chemical dynamics of molecules at an unprecedented resolution that is not possible with classical light.[1] Two-photon absorption (TPA) is the simplest spectroscopic technique that can demonstrate the merits of quantum light.[2−4] The entangled-photon pairs obtained by parametric down-conversion (PDC) have been employed in numerous TPA experiments.[5−12] The signal is commonly detected by the fluorescence from doubly excited molecular states.[6,13−15]

Most theoretical studies involving entangled photons are limited to the weak pump-field regime, which involves a single pair of entangled photons interacting with the molecule.[16−18] It is experimentally challenging to observe the weak spectroscopic signal generated by isolated entangled-photon pairs.[19−21] This difficulty may be overcome by increasing the pump intensity, whereby several entangled-photon pairs can interact with the molecule. One such example of the entangled-field is the bright-squeezed vacuum.[22] However, a strong pump increases unwanted contributions that arise from molecular interactions with photons belonging to different entangled pairs that lack the quantum information on the entangled field.

A spectroscopic signal generated by the bright squeezed vacuum can be divided into two parts, denoted as intermode and intramode contributions, where the former involves both the "signal" and the "idler" modes,[23] while the latter has only the "signal" or the "idler" mode contribution. Only the intermode part is sensitive to the photon entanglement. We have recently shown that at low pump intensities (but beyond single entangled-pair limit), the light-to-matter entanglement transfer is reduced by the presence of intramode contributions.[24] Recently, intense entangled beams have been employed in TPA[23] and virtual-state spectroscopy[25] to study the impact of time-entanglement between the two modes. The intramode contributions dominate at high pump intensities, which can obscure the quantum effects arising from the entangled nature of the field. This causes difficulties in observing the theoretically predicted effects of photon-entanglement in experiments. An accurate description of the entangled field effects, therefore, requires using arbitrary pump-pulse intensity (to enhance the signal) together with a spectroscopic scheme that can remove the unwanted background intramode contributions. This is the aim of the present work.

Received: February 18, 2025
Revised: April 16, 2025
Accepted: April 18, 2025
Published: April 30, 2025

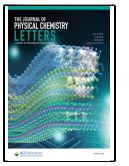

https://doi.org/10.1021/acs.jpclett.5c00518
J. Phys. Chem. Lett. 2025, 16, 4547−4554

A nonperturbative approach is used to describe the PDC process, which allows computing entangled fields induced by an arbitrarily strong pump pulse. The interaction of the pump-pulse and entangled fields with the PDC crystal is treated nonperturbatively. However, the interaction of the entangled fields with the sample is treated perturbatively. Starting with the effective Hamiltonian previously used by Dayan and Raymer[22,26] to study high pump-intensity effects, we derive a system of linear integro-differential equations whose solutions with appropriate boundary conditions provide the exact correlation functions of the entangled field. Our system of equations is equivalent to the one presented in Ref 27. Switching to the Wigner representation of the field correlation functions allows us to extend the exact analytical solutions for infinitely narrow spectral width pump (presented, e.g., in Ref 22) to obtain an asymptotically exact expression for the case of a narrow, rather than an infinitely narrow, pump. We compare the "almost analytical" Wigner approach with the results obtained from a completely numerical solution and (i) show that for a sufficiently narrow pump, the two methods show excellent agreement and (ii) identify the range of the pump spectral width, where the narrow pump solution can be safely implemented.

We use this approach to evaluate the Glauber's $g^{(2)}$ function of entangled photons, and study the role of entanglement-time and pump spectral width on the photon-statistics of the entangled field. We further investigate the TPA signal and its scaling with the pump intensity and spectral width. We finally propose an experimental protocol that can remove the unwanted intramode contributions from the TPA signal.

The TPA signal is given by the photon creation rate in the output (fluorescence) mode with frequency ω_f (see Section I in the SI)

$$R(\omega_f, t) \equiv \sum_\lambda \frac{d}{dt}\langle E_f^{\lambda\dagger}(t)E_f^{\lambda}(t)\rangle = \frac{2}{\hbar^2}\mathrm{Re}\sum_\lambda \sum_{i>j}\sum_{i'>j'} (\mu_{ij}\cdot\epsilon_\lambda)(\mu_{i'j'}^{*}\cdot\epsilon_\lambda)\int_{-\infty}^{t} d\tau \langle B_{ijR}^{\dagger}(t)B_{i'j'L}(\tau)\rangle e^{-i\omega_f(t-\tau)} \quad (1)$$

Here μ_{ij} is the transition dipole moment between molecular states i and j, and ϵ_λ is the output mode polarization. $B_{ij} = |j\rangle\langle i|$ is the excitation operator from the ith to jth electronic molecular state, and the subscripts R and L denote "right" and "left" superoperators, respectively, defined in Liouville space through their actions on the density-matrix, [e.g., $A_L\rho = A\rho$, $A_R\rho = \rho A$ such that $A_-\rho = (A_L - A_R)\rho$].[28] The angular bracket $\langle\cdot\rangle$ denotes the trace over the combined molecule and the incoming entangled field degrees-of-freedom.

Computing $R(\omega_f, t)$ requires calculating the exciton correlation function $\langle B_{ijR}^{\dagger}(t)B_{i'j'L}(\tau)\rangle$. This can be done by using a modified correlation $\mathcal{G}_{iji'j'}^{RL}(t,\tau) = \langle TB_{ijR}^{\dagger}(t)B_{i'j'L}(\tau)\rangle$, where T is the time-ordering operator. $R(\omega_f)$ depends on the retarded ($t > \tau$) correlation function. Calculating $\mathcal{G}_{iji'j'}^{RL}(t,\tau)$ requires computationally expensive solution of several self-consistent equations in terms of single-particle (Green's functions) propagators[28−30] for the molecule. In the following, we compute the exciton correlation function perturbatively in the (incoming) entangled field-molecule coupling by expressing the correlation function in the interaction picture.

$$\mathcal{G}_{iji'j'}^{RL}(t,\tau) = \left\langle TB_{ijR}^{\dagger}(t)B_{i'j'L}(\tau)e^{-i/\hbar\int d\tau_1 H_{int-}(\tau_1)}\right\rangle \quad (2)$$

with $H_{int}(t) = \sum_{ijq\lambda}\mu_{ij}B_{ij}^{\dagger}(t)E_q^{\lambda}(t) + h.c.$, where E_q^{λ} is the annihilation operator for the incoming field with frequency ω_q and polarization ϵ_λ. All time-dependences are in the interaction picture.

The zeroth-order contribution in the perturbative expansion of eq 2 in H_{int} vanishes for a molecule initially in the ground state. The two leading (second and fourth)-order contributions are

$$\begin{aligned}\mathcal{G}_{iji'j'}^{RL}(t,\tau) \approx{}& \frac{2}{\hbar^2}(\mu_{i_1j_1}\cdot\epsilon_{\lambda_1})(\mu_{i_2j_2}^{*}\cdot\epsilon_{\lambda_2})\int d\tau_1 d\tau_2\Big[\langle TE_{q_1L}^{\lambda_1}(\tau_1)E_{q_2R}^{\lambda_2\dagger}(\tau_2)\rangle\\ &\langle TB_{ijR}^{\dagger}(t)B_{i'j'L}(\tau)B_{i_1j_1L}^{\dagger}(\tau_1)B_{i_2j_2R}(\tau_2)\rangle\\ &+\frac{3}{\hbar^2}(\mu_{i_3j_3}^{*}\cdot\epsilon_{\lambda_3})(\mu_{i_4j_4}^{*}\cdot\epsilon_{\lambda_4})\int d\tau_3 d\tau_4\langle TE_{q_1L}^{\lambda_1}(\tau_1)E_{q_2L}^{\lambda_2}(\tau_2)E_{q_3R}^{\lambda_3\dagger}(\tau_3)E_{q_4R}^{\lambda_4\dagger}(\tau_4)\rangle\\ &\times\langle TB_{ijR}^{\dagger}(t)B_{i'j'L}(\tau)B_{i_1j_1L}^{\dagger}(\tau_1)B_{i_2j_2L}^{\dagger}(\tau_2)B_{i_3j_3R}(\tau_3)B_{i_4j_4R}(\tau_4)\rangle\\ &-\frac{6}{\hbar^2}(\mu_{i_3j_3}\cdot\epsilon_{\lambda_3})(\mu_{i_4j_4}^{*}\cdot\epsilon_{\lambda_4})\int d\tau_3 d\tau_4\\ &\times(\langle TE_{q_1L}^{\lambda_1}(\tau_1)E_{q_2L}^{\lambda_2}(\tau_2)E_{q_3L}^{\lambda_3\dagger}(\tau_3)E_{q_4R}^{\lambda_4\dagger}(\tau_4)\rangle\langle TB_{ijR}^{\dagger}(t)B_{i'j'L}(\tau)B_{i_1j_1L}^{\dagger}(\tau_1)\\ &B_{i_2j_2L}(\tau_2)B_{i_3j_3L}^{\dagger}(\tau_3)B_{i_4j_4R}(\tau_4)\rangle\\ &+\langle TE_{q_1L}^{\lambda_1}(\tau_1)E_{q_2R}^{\lambda_2}(\tau_2)E_{q_3R}^{\lambda_3\dagger}(\tau_3)E_{q_4R}^{\lambda_4\dagger}(\tau_4)\rangle\langle TB_{ijR}^{\dagger}(t)B_{i'j'L}(\tau)B_{i_1j_1L}^{\dagger}(\tau_1)\\ &B_{i_2j_2R}(\tau_2)B_{i_3j_3R}^{\dagger}(\tau_3)B_{i_4j_4R}(\tau_4)\rangle\Big]\end{aligned} \quad (3)$$

where summation over repeated indices is implied. Feynman diagrams associated with the physical processes that give rise to the various contributions in eq 3 are depicted in Figure 1.

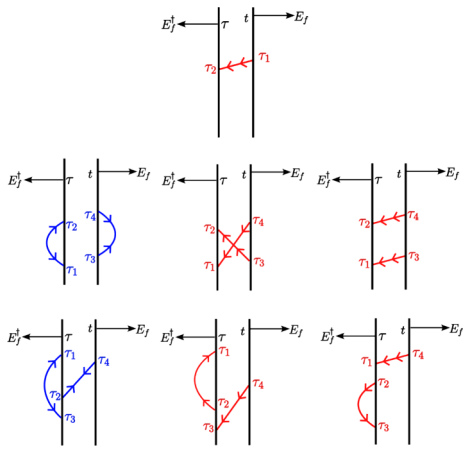

Figure 1. Diagrams contributing to the first term (top panel), the second term (middle panel), and the third term (bottom panel) in eq 3. Diagrams for the last term in eq 3 are obtained by interchanging the left and right interactions at τ_i, i = 1, 2, 3, 4, in the bottom diagram. Interactions at times t and τ represented by the horizontal arrows correspond to the observed fluorescent mode. Red (blue) curves with two arrowheads denote ordinary (anomalous), $D^{-+}(D^{--}, D^{+2})$ entangled-field propagators (see discussion below, eq 4). Arrowheads pointing inward (outward) the vertical black lines represent field E ($E^{\dagger}$).

The first term represents an excitation from the ground state $|g\rangle$ to the doubly excited state $|f\rangle$ by the absorption of a resonant pump photon, and the corresponding Feynman diagram is shown in Figure 1 (top). This contribution involves a two-point field propagator which is denoted by a double-arrow line connecting the two nodes at τ_1 and τ_2 in the Feynman diagram. This term could also represent absorption of a single "idler" or "signal" photon, which has the proper

https://doi.org/10.1021/acs.jpclett.5c00518
J. Phys. Chem. Lett. 2025, 16, 4547−4554

energy due to the finite pump-pulse bandwidth. The term also depends on the molecular dipole-correlation function which can be evaluated in terms of molecular parameters as discussed in Section II in the SI. Hereafter, we assume that the pump-photons in the crystal output are filtered out using phase-matching and do not contribute to the first term. Note that each field operator includes both the "signal" and "idler" modes, $E_q^\lambda = E_s^\lambda(\omega_q) + E_i^\lambda(\omega_q)$. The field correlation function $\langle TE_{q_1L}^{\lambda_1}(\tau_1)E_{q_2R}^{\lambda_2\dagger}(\tau_2)\rangle$ (Section III in the SI) has four terms, where two cross terms that contain intermode correlations vanish. Thus, the first term in eq 3 only includes intramode photon correlations which is nonzero if the polarizations (ϵ_{λ_1} and ϵ_{λ_2}) are parallel.

The second and the third terms in eq 3 contain four-time field propagators that, by using Wick's theorem for Boson fields, may be factorized into products of two-time field propagators.

$$
\begin{aligned}
&D_{\lambda_1\lambda_2\lambda_3\lambda_4}^{--++LLLR}(\tau_1, \tau_2, \tau_3, \tau_4)\\
&= \langle TE_{q_1L}^{\lambda_1}(\tau_1)E_{q_2L}^{\lambda_2}(\tau_2)E_{q_3L}^{\lambda_3\dagger}(\tau_3)E_{q_4R}^{\lambda_4\dagger}(\tau_4)\rangle\\
&= \langle TE_{q_1L}^{\lambda_1}(\tau_1)E_{q_2L}^{\lambda_2}(\tau_2)\rangle\langle TE_{q_3L}^{\lambda_3\dagger}(\tau_3)E_{q_4R}^{\lambda_4\dagger}(\tau_4)\rangle\\
&\quad + \langle TE_{q_1L}^{\lambda_1}(\tau_1)E_{q_3L}^{\lambda_3\dagger}(\tau_3)\rangle\langle TE_{q_2L}^{\lambda_2}(\tau_2)E_{q_4R}^{\lambda_4\dagger}(\tau_4)\rangle\\
&\quad + \langle TE_{q_1L}^{\lambda_1}(\tau_1)E_{q_4R}^{\lambda_4\dagger}(\tau_4)\rangle\langle TE_{q_2L}^{\lambda_2}(\tau_2)E_{q_3L}^{\lambda_3\dagger}(\tau_3)\rangle
\end{aligned}
\tag{4}
$$

where a "−(+)" sign on the propagator D denotes that the corresponding field operator is $E(E^\dagger)$, for example, $D^{-+}(t, t') = \langle TE(t)E^\dagger(t')\rangle$. The first term in eq 4 is nonzero only when the paired modes, (q_1, q_2) and (q_3, q_4), are different "signal" and "idler" modes. This contribution, therefore, depends on intermode correlations and carries information on the quantum state of both modes. The other two terms survive only when both paired modes belong to the same mode and represent intramode field correlations. Feynman diagrams corresponding to the second and the third terms in eq 3 are shown in the middle and the bottom panels in Figure 1. Each term is represented by three Feynman diagrams, and each diagram consists of two field propagators.

We consider the molecular level-scheme depicted in Figure 2, which consists of a ground state $|g\rangle$, one doubly excited state $|f\rangle$, and three intermediate singly excited states $|e_i\rangle$, i = 1, 2, 3.

Signals arising from the various processes depicted in Figure 1 are computed by expanding the molecular correlation functions in eq 3 in molecular eigenstates, as discussed in Section II in the SI. The leading-order term, given by the first diagram in Figure 1, originates from intramode interactions. The other terms contain both the inter- and the intramode contributions, represented by the blue and the red colored field propagators, respectively. These field propagators are computed using the effective Hamiltonian approach given in Section III in the SI. The different contributions, $R^{(n)}$, given in eqs 5−10 in the SI, therefore, carry quantum information regarding the entangled light field and are related to Glauber's $g^{(2)}$ function which is commonly used to describe the nonclassical behavior of light.[31] $g^{(2)}(t, \tau)$ can be measured by the coincidence-counting of photons at times $t - \tau$ and t

$$
g^{(2)}(t, \tau) = \frac{\langle E^\dagger(t-\tau)E^\dagger(t)E(t)E(t-\tau)\rangle}{\langle E^\dagger(t-\tau)E(t-\tau)\rangle\langle E^\dagger(t)E(t)\rangle} \tag{5}
$$

Integrating over t gives

$$
g^{(2)}(\tau) = \frac{1}{S(\tau)}\int\int\int \frac{d\omega_1 d\omega_2 d\omega_3}{(2\pi)^3} e^{-i(\omega_2-\omega_3)\tau}\langle E^\dagger(\omega_1)E^\dagger(\omega_2)E(\omega_3)E(\omega_1+\omega_2-\omega_3)\rangle \tag{6}
$$

where $\omega_4 = \omega_1 + \omega_2 - \omega_3$ and $S(\tau) = \int \frac{d\omega_1 d\omega_2 d\omega_3}{(2\pi)^3}\langle E^\dagger(\omega_1)E(\omega_4)\rangle\langle E^\dagger(\omega_2)E(\omega_3)\rangle e^{-i(\omega_2-\omega_3)\tau}$ is a normalization factor that only includes the intramode field correlations. $g^{(2)}$ can be decomposed into a sum of intramode, $g_0^{(2)}$, and intermode, $g_1^{(2)}$, contributions. Both contributions decay with τ. At long τ, the normalized intramode part saturates to unity, while the intermode part vanishes.

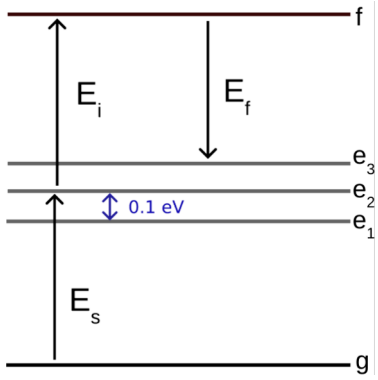

Figure 2. Energy level scheme used in our simulations with energies $\mathcal{E}_g$ = 0 fs^{-1}, $\mathcal{E}_{e1}$ = 1.9 fs^{-1}, $\mathcal{E}_{e2}$ = 2 fs^{-1}, $\mathcal{E}_{e3}$ = 2.1 fs^{-1}, and $\mathcal{E}_f$ = 4 fs^{-1} after subtracting the zero-point energy.

The inter- and intramode components of $g^{(2)}(\tau)$ for various field entanglement times are displayed in Figure 3. Both components show strong dependence on the entanglement time and rapidly decay as the entanglement time is decreased. At high pump intensities, the two contributions are virtually identical. However, differences show up at low pump intensities where the intermode contribution survives for longer delays and vanishes beyond the entanglement time. For a degenerate entangled field produced by a continuous laser field, the Glauber function is computed in Section III−B in the SI. The temporal profile of $g_{0/1}^{(2)}(\tau)$ is Gaussian with a time-scale, which is mainly determined by the entanglement time for low-pump intensities, while, at larger intensities, it decreases with the intensity, leading to a shorter effective entanglement time. The analytic results for the continuous field can be extended for a finite (nonzero) but large time-scale (narrow bandwidth) pump pulse using Wigner representation as discussed in Section III in the SI. The inset in Figure 3 compares the numerical results with the semianalytical (Wigner) results for σ_p = 0.3 fs^{-1}.

The time-dependent Glauber function is depicted for different pump bandwidths in Figure 4. At high pump intensities, as the bandwidth is increased, the relaxation slows down, implying a longer effective entanglement time. The difference between the intra- and intermode components is more pronounced at low pump intensities. The relaxation of the intermode contribution strongly depends on the

https://doi.org/10.1021/acs.jpclett.5c00518
J. Phys. Chem. Lett. 2025, 16, 4547−4554

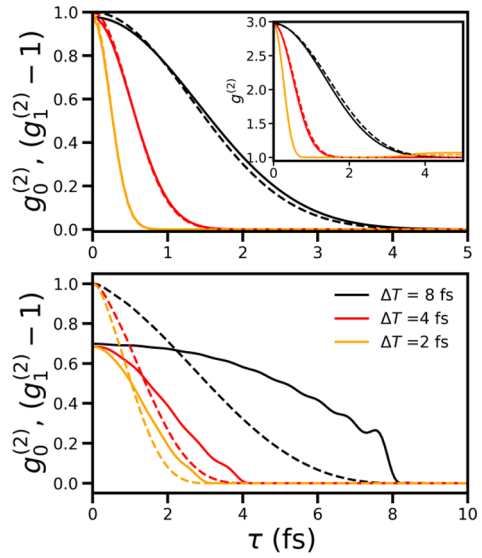

Figure 3. Time-dependence of the intermode ($g_1^{(2)}$, solid) and intramode ($g_0^{(2)} - 1$, dashed) parts of $g^{(2)}(\tau)$ for different entanglement times is shown. Upper (lower) panel: for high (low) pump intensity, $I_p = 5.4 \times 10^9$ (5.4×10^7) W/cm^2. Other parameters are $\sigma_p = 0.3$ fs^{-1}, $\omega_p = 4$ fs^{-1}, $\omega_s = 2$ fs^{-1}, and PDC crystal length $l = 20$ μm. The inset compares the $g^{(2)}(\tau)$ function calculated numerically (solid) with the semianalytical (dashed) solution.

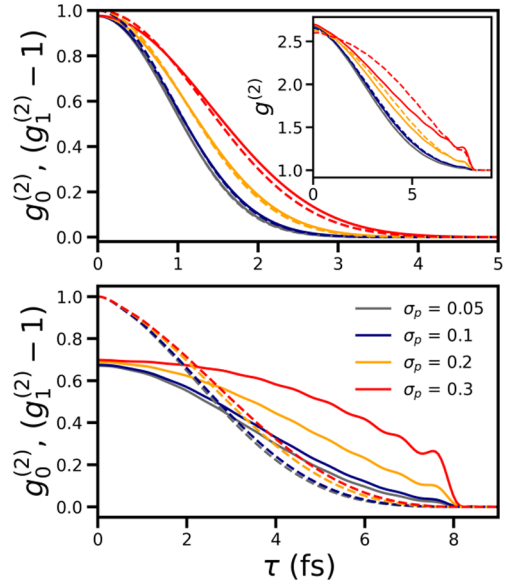

Figure 4. Time-dependence of the intermode ($g_1^{(2)}$, solid) and the intramode ($g_0^{(2)}$, dashed) contributions for different pulse bandwidths σ_p. The upper (lower) panel shows the intermode and intramode contributions for a strong (weak) pump with the field strength of $I_p = 5.4 \times 10^9$ (5.4×10^7) W/cm^2 for the entanglement time $\Delta T = 8$ fs. The inset compares the total $g^{(2)}$ calculated numerically (solid) with semianalytical results (dashed) for $I_p = 5.4 \times 10^7$ W/cm^2.

bandwidth, which is qualitatively different from the intense-pump case. As the bandwidth is increased, it shows weaker dependence on τ for τ smaller than the entanglement time, and vanishes for larger τ. The relaxation in the intramode part also slows down with increased bandwidth but remains qualitatively the same as for the intense pump. Thus, the intermode part of the Glauber function directly reveals information on the field entanglement time at larger bandwidths and low pump intensities. The inset compares the numerical and the semianalytical results for a finite bandwidth pump. The exact numerical method and the semianalytical Wigner approach agree well for small $\sigma_p \Delta T < 0.2$.

Having discussed the statistical properties of the entangled field, we now turn to the TPA process, detected by fluorescence. All processes depicted in Figure 1 generally contribute to the signal. To simplify the analysis, we focus on a narrow-band pump resonant with the doubly excited state of the molecule. The "signal" and "idler" photon energies are bounded by the double-excitation energy. The doubly excited state population is generated by absorbing the "signal" and "idler" photons and the fluorescence is given by the $R^{(2)}$ term in eq 6 of the SI, the corresponding diagrams are given in the second row in Figure 1. Radiative transitions $|f\rangle \rightarrow |e\rangle$ and $|f\rangle \rightarrow |g\rangle$ contribute to the fluorescence from the double-excited state. Note that when the transition dipole μ_{fg} vanishes, the fluorescence solely comes from the transition $|f\rangle \rightarrow |e\rangle$ in $R^{(2)}$.

To study the scaling with the pump intensity, we consider a case where both "signal" and "idler" modes have both vertical and horizontal polarizations with equal magnitudes and all molecular transition dipoles are aligned by 45° angle to both directions so that $\mathcal{M}$ in eq 6 in the SI is independent of the field polarization. All terms in $R^{(2)}$ obtained after interchanging polarizations then make the same contribution as the first term in $R^{(2)}$ and we can drop the polarization subscripts. The renormalized signal $\tilde{R}(\omega_f) = \mathrm{Re}\{R^{(2)}(\omega_f)/\mathcal{M}^{fe_1;fe_1;fe;eg;e'g;fe'}\}$ is given by

$$\tilde{R}(\omega_f) = \mathrm{Im} \int \frac{d\omega_1 d\omega_2 d\omega_3}{(2\pi)^3} \frac{(48/\hbar^6) D(\omega_1, \omega_2, \omega_3, \omega_1 + \omega_2 - \omega_3)}{|\omega_1 + \omega_2 - \mathcal{E}_{fg} + i\eta|^2 (\omega_2 - \mathcal{E}_{eg} + i\eta)(\omega_3 - \mathcal{E}_{e'g} - i\eta)(\omega_f - \omega_1 - \omega_2 + \mathcal{E}_{jg} - i\eta)} \tag{7a}$$

https://doi.org/10.1021/acs.jpclett.5c00518
J. Phys. Chem. Lett. 2025, 16, 4547−4554

where from eq 4

$$D(\omega_1, \omega_2, \omega_3, \omega_4) = \sum_{qq'=i,s} \langle E_q^\dagger(\omega_3) E_q(\omega_1)\rangle \langle E_{q'}^\dagger(\omega_4) E_{q'}(\omega_2)\rangle + (\omega_1 \Leftrightarrow \omega_2) + \sum_{q\neq q'=i,s} \sum_{q_1\neq q_1'=i,s} \langle E_q(\omega_1) E_{q'}(\omega_2)\rangle \langle E_q^\dagger(\omega_3) E_{q_1'}^\dagger(\omega_4)\rangle \tag{7b}$$

For a weak pump, where only a single entangled-photon pair interacts with the molecule, only the last term in eq 7b survives. The first two terms, therefore, represent intramode contributions corresponding to the two rightmost diagrams in the middle panel in Figure 1.

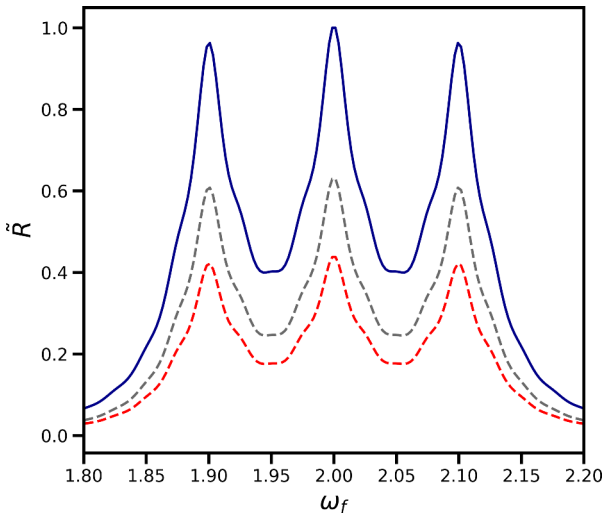

Figure 5. Normalized TPA signal from the model molecule (eq 7a). The dashed-red (gray) curve is the intermode contribution for I_p = 5.41×10^7 (1.35×10^7) W/cm^2. Here, σ_p = 0.1 fs^{-1}, η = 0.015, and T_e = 13.33 fs.

Figure 5 depicts $\tilde{R}(\omega_f)$ for a model molecule with one $|f\rangle$ state and three singly excited states having energies E_f = 4 fs^{-1}, E_{e1} = 1.9 fs^{-1}, E_{e_2} = 2.0 fs^{-1}, E_{e3} = 2.1 fs^{-1} above the ground state $|g\rangle$. The three peaks represent transitions from $|f\rangle$ to the three intermediate states. The intermode contribution is shown by the dashed curves for two different pump intensities. The relative weight of the intermode contribution depends on the pump amplitude and grows as the pump intensity is decreased. This is because the probability that the molecule interacts with two photons of an entangled-pair increases at lower intensities.

The variation of the TPA signal with the pump intensity is shown in Figure 6. The pump-intensity is given by $I_p = c\epsilon_0 n_p |E_p|^2/2$, where E_p is the pump pulse amplitude, and n_p is the refractive index of the PDC crystal for the pump-pulse, c is the speed of light, and ϵ_0 is the permittivity of free space, at the resonant frequency ω_s = 2.0 fs^{-1}.

The intermode contributions grow linearly over a wide range of pump intensity and dominates over the intramode contributions that grow quadratically. However, for larger intensities, both contributions grow nonlinearly, while the intermode contribution remains higher. With an increase in the bandwidth, the TPA cross-section decreases while the intensity range for which intermode contribution dominates increases by up to 1 order of magnitude. PDC parameters for the

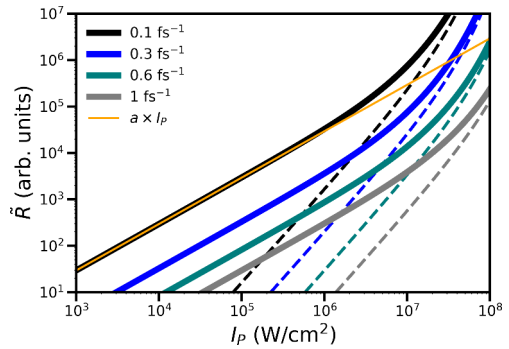

Figure 6. Variation of the TPA signal for ω_f = 2 fs^{-1} with pump-field intensity. The curves (top to bottom) denote the total signal calculated using eq 7a for pump band-widths σ_p = 0.1 fs^{-1}, 0.3 fs^{-1}, 0.6 fs^{-1}, and 1.0 fs^{-1}, respectively. The dashed curves show intramode contributions. The orange line is the fit for a = 0.03. The entanglement time is T_e = 13.33 fs, $\bar{n}_s = \bar{n}_i$ = 2.24, n_p = 2.361, and $\chi^{(2)}_{eff}$ = 4.6 pm/V.

$LiNbO_3$ are considered in calculating the TPA signal.[32] The refractive indices for the considered photon frequencies in the PDC crystal are obtained following the procedure in Ref 33. The value of the pump intensity beyond which nonlinear effects become significant for three commonly used PDC crystals at different pump spectral widths are given in the Table 1.

The intermode contributions carry the quantum nature of light and reveal the nonclassical response of molecules. For example, information regarding the entanglement time is contained in the intermode field correlations which probes the linear variation of the TPA signal over a large intensity range. These contributions dominate at lower pump intensities but are masked by intramode processes at higher intensities, making it hard to take full advantage of the quantum light. In the next section, we propose a setup that removes the intramode contributions at all pump intensities.

We now present a model experimental setup that can help filter out the unwanted (classical) intramode contributions from the TPA signal. The inter- and intramode processes have different contributions, as shown in Figure 5 and 6, and the latter dominates at higher pump intensities. Thus, in order to take a complete advantage of the quantum nature of the entangled light, these contributions should be removed.

The intermode contribution to the signal only appears when the "signal" and "idler" modes are entangled to each other, and it vanishes for light fields that lack such quantum correlation in different modes. The intramode contribution, on the other hand, shows a direct frequency correlation between the involved modes. Therefore, one can use two distinct classically correlated pulses such that the intramode contribution is intact while the intermode contribution vanishes, and the resulting signal can be subtracted from the entangled TPA signal to obtain the quantum part. However, two conditions must be satisfied: Bandwidths and the statistics (as determined by Glauber function) of the uncorrelated "signal" and "idler" modes must be the same as obtained from the actual PDC process. The simplest way to achieve this would be by utilizing two identical PDC crystals to generate statistically identical pairs of "signal" and "idler" pulses. We then select the "signal" pulse from one pair and the "idler" pulse from the other pair. These pulses are obviously not entangled, but are statistically identical to the entangled pulses and, upon interaction with the

https://doi.org/10.1021/acs.jpclett.5c00518
J. Phys. Chem. Lett. 2025, 16, 4547−4554

Table 1. Pump Intensities (in W/cm^2) at which Linear-to-Nonlinear Crossover Appears for Different Crystals and Pulse Widths

crystal	0.1 (fs^{-1})	0.3 (fs^{-1})	0.6 (fs^{-1})	1 (fs^{-1})
$LiNbO_3$ (n_i = 2.24, n_p = 2.36, $\chi^{(2)}_{eff}$ = 4.6 pm/V)	8×10^5	2×10^6	4×10^6	6×10^6
$KNbO_3$ (n_i = 2.13,n_p = 2.24, $\chi^{(2)}_{eff}$ = 10.8 pm/V)	1.23×10^5	3.07×10^5	6.13×10^5	9.21×10^5
$LiTaO_3$ (n_i = 2.14,n_p = 2.23, $\chi^{(2)}_{eff}$ = 0.85 pm/V)	2×10^7	5.03×10^7	1×10^8	1.51×10^8

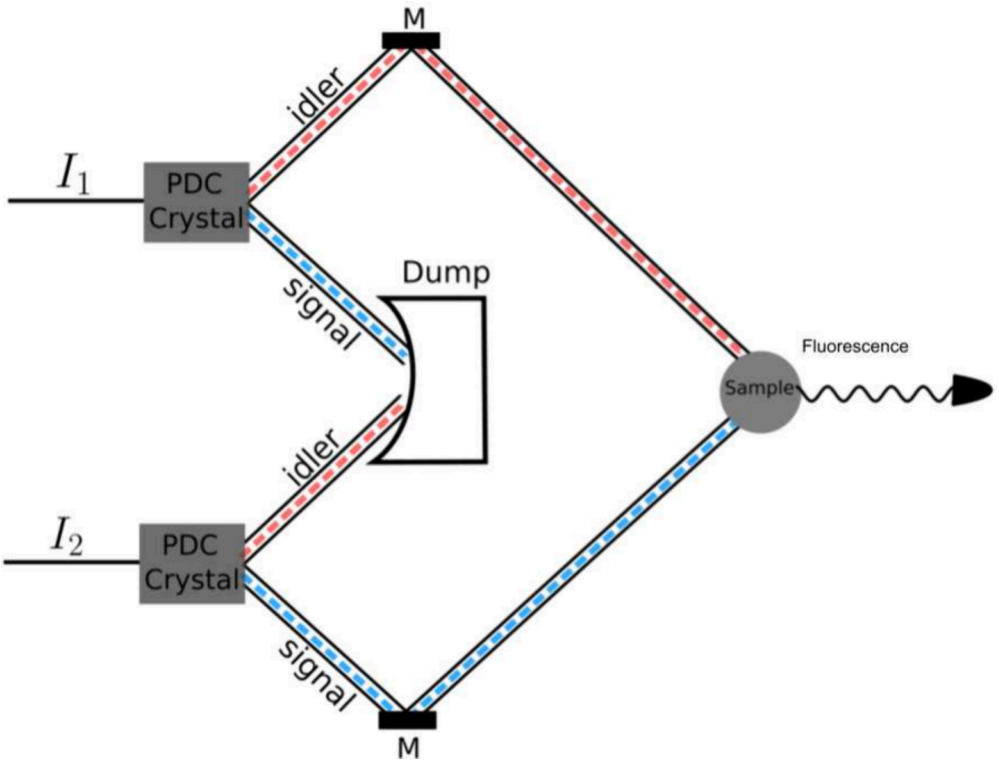

Figure 7. Schematic setup that can be used to generate TPA signal that only includes intramode contributions. The "signal" and "idler" photons from two different entangled-photon pairs are utilized. The use of an identical pump and the PDC crystal ensure the generated entangled-photon pairs are statistically identical to those generated by a single PDC crystal but uncorrelated.

molecule, generate the signal, as depicted schematically in Figure 7. This signal will only have the intramode contributions since the two modes are not correlated. The signal due to intermode contributions is obtained by subtracting this signal from the total signal generated using entangled light, i.e., the signal measured in the presence of only one of the PDC crystals.

Two-photon absorption with an entangled-photon field is a weak process. The advantage of entangled light is limited to lower pump intensities where contribution from interaction with entangled photons can outweigh contribution from nonentangled photons by orders of magnitude. This range of pump intensities can be enhanced by using a pump-pulse with a broader bandwidth, at the cost of signal intensity. At higher intensities, both contributions are almost equal but can be separated using the proposed experimental scheme.

Finally, we note that (i) the effective Hamiltonian used in the present study and elsewhere[22,26] can be derived in a clean way from an effective action of the low-frequency electromagnetic (EM) field for strong pump (the weak pump perturbative expansion of the effective action has been introduced in Ref 16) by considering the complete perturbative expansion for the solution of the Dyson equation and neglecting the fast-oscillating (non-RWA) terms, whose contributions can be neglected. (ii) By applying the Kirchhoff-integral approach to the correlation functions of the field, together with the semiclassical (in linear optics known as eikonal) expressions for the Green functions of the Maxwell equations, one can explicitly express the entangled field correlation functions at the experimental sample in terms of their at-the-PDC-crystal counterpart, with those expressions carefully describing the optical experimental setup, e.g., lenses, mirrors, delay lines, etc., thus providing the actual values (including prefactors) of the measured signal. However, the aforementioned results go beyond the scope of this paper and will be addressed elsewhere.

■ ASSOCIATED CONTENT

Data Availability Statement

Data underlying the results presented in this paper are not publicly available at this time but may be obtained from the authors upon reasonable request.

Supporting Information

The Supporting Information is available free of charge at https://pubs.acs.org/doi/10.1021/acs.jpclett.5c00518.

Effective Hamiltonian approach used in high-gain PDC process, signal derivations, and frequency-dispersed two-point field correlators for different pump-pulse parameters (PDF)

https://doi.org/10.1021/acs.jpclett.5c00518
J. Phys. Chem. Lett. 2025, 16, 4547−4554

AUTHOR INFORMATION

Corresponding Author

Shaul Mukamel − *Department of Chemistry and Department of Physics and Astronomy, University of California, Irvine, California 92614, United States;* orcid.org/0000-0002-6015-3135; Email: smukamel@uci.edu

Authors

Deependra Jadoun − *Department of Chemistry and Department of Physics and Astronomy, University of California, Irvine, California 92614, United States;* orcid.org/0000-0003-3305-9140

Upendra Harbola − *Department of Inorganic and Physical Chemistry, Indian Institute of Science, Bangalore 560012, India;* orcid.org/0000-0003-4053-8641

Vladimir Y. Chernyak − *Department of Chemistry, Wayne State University, Detroit, Michigan 48202, United States; Department of Mathematics, Wayne State University, Detroit, Michigan 48202, United States*

Complete contact information is available at: https://pubs.acs.org/10.1021/acs.jpclett.5c00518

Notes

The authors declare no competing financial interest.

ACKNOWLEDGMENTS

We thank Victor M. Freixas for the helpful discussion, and Austin T. Green for helping with the TOC graphic. U.H. acknowledges support from the Science and Engineering Research Board, India, under Grant No. CRG/2020/0011100 and the Fulbright-Nehru Academic and Excellence Fellowship, 2023-24, sponsored by the U.S. Department of State and the United State-India Education Foundation. V.Y.C. and S.M. gratefully acknowledge the support of the U.S. Department of Energy, Office of Science, Basic Energy Sciences Award DES0022134, which has primarily funded this work. S.M. gratefully acknowledges the support of the National Science Foundation through Grant No. CHE-2246379. S.M. gratefully acknowledges support from the Department of Energy through Grant no. DE-SC0023233.

REFERENCES

(1) Mukamel, S.; Freyberger, M.; Schleich, W.; Bellini, M.; Zavatta, A.; Leuchs, G.; Silberhorn, C.; Boyd, R. W.; Sánchez-Soto, L. L.; Stefanov, A.; et al. Roadmap on quantum light spectroscopy. *J. Phys. B: At. Mol. Opt.* **2020**, *53*, 072002.

(2) Gilles, L.; Knight, P. Two-photon absorption and nonclassical states of light. *Phys. Rev. A* **1993**, *48*, 1582.

(3) Gea-Banacloche, J. Two-photon absorption of nonclassical light. *Phys. Rev. Lett.* **1989**, *62*, 1603.

(4) Landes, T.; Raymer, M. G.; Allgaier, M.; Merkouche, S.; Smith, B. J.; Marcus, A. H. Quantifying the enhancement of two-photon absorption due to spectral-temporal entanglement. *Opt. Express* **2021**, *29*, 20022−20033.

(5) Parzuchowski, K. M.; Mikhaylov, A.; Mazurek, M. D.; Wilson, R. N.; Lum, D. J.; Gerrits, T.; Camp, Jr. C. H.; Stevens, M. J.; Jimenez, R. Setting bounds on entangled two-photon absorption cross sections in common fluorophores. *Phys. Rev. Applied* **2021**, *15*, 044012.

(6) Lee, D.-I.; Goodson, T. Entangled photon absorption in an organic porphyrin dendrimer. *J. Phys. Chem. B* **2006**, *110*, 25582−25585.

(7) Upton, L.; Harpham, M.; Suzer, O.; Richter, M.; Mukamel, S.; Goodson, T. Optically excited entangled states in organic molecules illuminate the dark. *J. Phys. Chem. Lett.* **2013**, *4*, 2046−2052.

(8) Varnavski, O.; Pinsky, B.; Goodson, T. Entangled photon excited fluorescence in organic materials: an ultrafast coincidence detector. *J. Phys. Chem. Lett.* **2017**, *8*, 388−393.

(9) Harpham, M. R.; Suzer, O.; Ma, C.-Q.; Bauerle, P.; Goodson, T. Thiophene dendrimers as entangled photon sensor materials. *J. Am. Chem. Soc.* **2009**, *131*, 973−979.

(10) Hickam, B. P.; He, M.; Harper, N.; Szoke, S.; Cushing, S. K. Single-photon scattering can account for the discrepancies among entangled two-photon measurement techniques. *J. Phys. Chem. Lett.* **2022**, *13*, 4934−4940.

(11) Corona-Aquino, S.; Calderón-Losada, O.; Li-Gómez, M. Y.; Cruz-Ramirez, H.; Álvarez-Venicio, V.; Carreon-Castro, M. D. P.; de J León-Montiel, R.; U'Ren, A. B. Experimental study of the validity of entangled two-photon absorption measurements in organic compounds. *J. Phys. Chem. A* **2022**, *126*, 2185−2195.

(12) Tabakaev, D.; Montagnese, M.; Haack, G.; Bonacina, L.; Wolf, J.-P.; Zbinden, H.; Thew, R. Energy-time-entangled two-photon molecular absorption. *Phys. Rev. A* **2021**, *103*, 033701.

(13) Guzman, A. R.; Harpham, M. R.; Suzer, O.; Haley, M. M.; Goodson, T. G. Spatial control of entangled two-photon absorption with organic chromophores. *J. Am. Chem. Soc.* **2010**, *132*, 7840−7841.

(14) Tabakaev, D.; Djorović, A.; La Volpe, L.; Gaulier, G.; Ghosh, S.; Bonacina, L.; Wolf, J.-P.; Zbinden, H.; Thew, R. Spatial properties of entangled two-photon absorption. *Phys. Rev. Lett.* **2022**, *129*, 183601.

(15) Landes, T.; Allgaier, M.; Merkouche, S.; Smith, B. J.; Marcus, A. H.; Raymer, M. G. Experimental feasibility of molecular two-photon absorption with isolated time-frequency-entangled photon pairs. *Phys. Rev. Res.* **2021**, *3*, 033154.

(16) Kizmann, M.; Yadalam, H. K.; Chernyak, V. Y.; Mukamel, S. Quantum interferometry and pathway selectivity in the nonlinear response of photosynthetic excitons. *Proc. Natl. Acad. Sci. U.S.A.* **2023**, *120*, No. e2304737120.

(17) Villabona-Monsalve, J. P.; Calderón-Losada, O.; Nuñez Portela, M.; Valencia, A. Entangled two photon absorption cross section on the 808 nm region for the common dyes zinc tetraphenylporphyrin and rhodamine b. *J. Phys. Chem. A* **2017**, *121*, 7869−7875.

(18) Gea-Banacloche, J. Two-photon absorption of nonclassical light. *Phys. Rev. Lett.* **1989**, *62*, 1603.

(19) Landes, T.; Smith, B. J.; Raymer, M. G. Limitations in fluorescence-detected entangled two-photon-absorption experiments: Exploring the low-to high-gain squeezing regimes. *Phys. Rev. A* **2024**, *110*, 033708.

(20) Raymer, M. G.; Landes, T.; Marcus, A. H. Entangled two-photon absorption by atoms and molecules: A quantum optics tutorial. *J. Chem. Phys.* **2021**, *155*, 081501.

(21) Mikhaylov, A.; Wilson, R. N.; Parzuchowski, K. M.; Mazurek, M. D.; Camp Jr, C. H.; Stevens, M. J.; Jimenez, R. Hot-band absorption can mimic entangled two-photon absorption. *J. Phys. Chem. Lett.* **2022**, *13*, 1489−1493.

(22) Raymer, M. G.; Landes, T. Theory of two-photon absorption with broadband squeezed vacuum. *Phys. Rev. A* **2022**, *106*, 013717.

(23) Svozilík, J.; Peřina Jr, J.; León-Montiel, R. d. J. Two-photon absorption spectroscopy using intense phase-chirped entangled beams. *Chem. Phys.* **2018**, *510*, 54−59.

(24) Harbola, U.; Candelori, L.; Klein, J. R.; Chernyak, V. Y.; Mukamel, S. Two-qubit-entanglement in matter created by entangled-photon pairs: A perturbative analysis. *AVS Quantum Sci.* **2024**, *6*, 031402.

(25) Svozilík, J.; Peřina, J.; León-Montiel, R. d. J. Virtual-state spectroscopy with frequency-tailored intense entangled beams. *J, Opt. Soc. Am. B* **2018**, *35*, 460−467.

(26) Dayan, B. Theory of two-photon interactions with broadband down-converted light and entangled photons. *Phys. Rev. A* **2007**, *76*, 043813.

(27) Christ, A.; Brecht, B.; Mauerer, W.; Silberhorn, C. Theory of quantum frequency conversion and type-II parametric down-conversion in the high-gain regime. *New J. Phys.* **2013**, *15*, 053038.

(28) Harbola, U.; Mukamel, S. Superoperator nonequilibrium Green's function theory of many-body systems; applications to charge transfer and transport in open junctions. *Phys. Rep.* **2008**, *465*, 191−222.
(29) Onida, G.; Reining, L.; Rubio, A. Electronic excitations: density-functional versus many-body Green's-function approaches. *Rev. Mod. Phys.* **2002**, *74*, 601.
(30) Harbola, U.; Mukamel, S. Nonequilibrium superoperator GW equations. *J. Chem. Phys.* **2006**, *124*, 044106.
(31) Glauber, R. J. The quantum theory of optical coherence. *Phys. Rev.* **1963**, *130*, 2529.
(32) Shoji, I.; Kondo, T.; Kitamoto, A.; Shirane, M.; Ito, R. Absolute scale of second-order nonlinear-optical coefficients. *J. Opt. Soc. Am. B* **1997**, *14*, 2268−2294.
(33) Edwards, G.; Lawrence, M. A temperature-dependent dispersion equation for congruently grown lithium niobate. *Opt. Quant. Electron.* **1984**, *16*, 373−375.

https://doi.org/10.1021/acs.jpclett.5c00518
J. Phys. Chem. Lett. 2025, 16, 4547−4554

Supporting Information: Pump-intensity-scaling of Two-photon Absorption and Photon Statistics of Entangled-photon Fields

Deependra Jadoun,[†,‡] Upendra Harbola,[¶] Vladimir Y. Chernyak,[§,‖] and Shaul Mukamel[*,†,‡]

†*Department of Chemistry, University of California, Irvine, CA 92614, USA*

‡*Department of Physics and Astronomy, University of California, Irvine, CA 92614, USA*

¶*Department of Inorganic and Physical Chemistry, Indian Institute of Science, Bangalore 560012, India*

§*Department of Chemistry, Wayne State University, 5101 Cass Ave, Detroit, Michigan 48202, USA*

‖*Department of Mathematics, Wayne State University, 656 W. Kirby, Detroit, Michigan 48202, USA*

E-mail: smukamel@uci.edu

Derivation of Eq. 1 in the main text

The molecular system interacting with the radiation field is represented by the Hamiltonian,

$$H = \sum_i \mathcal{E}_i B_{ii} + \sum_s \hbar\omega_s E_s^\dagger E_s + \sum_{s,i>j} (\mu_{ij}^s B_{ij}^\dagger E_s + h.c.) + \mathcal{H} \tag{1}$$

where $\mathcal{E}_i$ is the energy of the ith molecular state $|i\rangle$, $B_{ij} = |j\rangle\langle i|$ is the exciton operator, μ_{ij} is the transition dipole-matrix element between states $|i\rangle$ and $|j\rangle$, $E_s^\dagger(E_s)$ is the boson creation (annihilation) operator for the detected (fluorescence) field mode with frequency ω_s. The third term represents interaction of the detected mode with the molecule, and the last term is the Hamiltonian of the incoming field that prepares the electronic excitation and its interaction with the molecule. In our simulations, we assume an entangled-photon field described by Hamiltonian $\mathcal{H}$ which needs not be specified at this point.

The signal is defined by the rate of change of intensity in the detected mode ω_s, and it can be solved using the Heisenberg's equation of motion,

$$R(\omega_s, t) \;=\; \frac{d}{dt}\langle E_s^\dagger(t)E_s(t)\rangle = \frac{i}{\hbar}\langle[H, E_s^\dagger(t)E_s(t)]\rangle = -\frac{2}{\hbar}\,\mathrm{Im}\,\sum_{i>j}\mu_{ij}^s\langle B_{ij}^\dagger(t)E_s(t)\rangle \qquad (2)$$

where $\langle\cdot\rangle$ denotes average over the full Hilbert space of H. We assume weak interaction with the detected mode and compute the correlation $\langle B_{ij}^\dagger(t)E_s(t)\rangle$ to the leading order in the light-matter interaction. This gives,

$$\langle B_{ij}^\dagger(t)E_s(t)\rangle = \frac{-i}{\hbar}\sum_{i'<j'}\mu_{i'j'}^{s'}\int_{-\infty}^{t} d\tau\langle B_{ij}^\dagger(t)B_{i'j'}^\dagger(\tau)\rangle\langle E_s(t)E_{s'}^\dagger(\tau)\rangle, \qquad (3)$$

where the time evolution is now in the interaction picture, and molecular operators evolve with the Hamiltonian $\sum_i \mathcal{E}_i B_{ii} + \mathcal{H}$ while the field operators evolve with free-field Hamiltonian, $E_s(t) = E_s e^{-i\omega_s t}$, leading to $\langle E_s(t)E_{s'}^\dagger(\tau)\rangle = \delta_{ss'}e^{-i\omega(t-\tau)}$. Substituting this in Eq. (3), Eq. (2) finally results in Eq. 1 of the main text.

Contributions of the diagrams given in Fig. 1

For a fixed time ordering $\tau_1 > \tau_2 > \tau_3 > \tau_4$, different dipole correlations can be evaluated in terms of molecular state energies. Since these correlation functions require taking trace with respect to the ground state of the isolated molecule, we can use, $B_{ij}(t) = e^{-i\mathcal{E}_{ij}t}|j\rangle\langle i|$.

Thus, for example, the following matter correlation function can be evaluated as follows,

$$\begin{aligned}
&\langle B^\dagger_{ijR}(t)B_{i'j'L}(\tau)B^\dagger_{i_1j_1L}(\tau_1)B_{i_2j_2R}(\tau_2)\rangle \equiv \langle B_{i_2j_2}(\tau_2)B^\dagger_{ij}(t)B_{i'j'}(\tau)B^\dagger_{i_1j_1}(\tau_1)\rangle \\
= \;& \langle g|j_2\rangle\langle i_2|i\rangle\langle j|j'\rangle\langle i'|i_1\rangle\langle j_1|g\rangle e^{i\mathcal{E}_{ij}t}e^{-i\mathcal{E}_{i'j'}\tau}e^{-i\mathcal{E}_{i_2j_2}\tau_2}e^{i\mathcal{E}_{i_1j_1}\tau_1} \\
= \;& \delta_{jj'}\delta_{ii_2}\delta_{i'i_1}\delta_{j_1g}\delta_{j_2g}e^{i\mathcal{E}_{ij}t}e^{-i\mathcal{E}_{i'j'}\tau}e^{-i\mathcal{E}_{i_2j_2}\tau_2}e^{i\mathcal{E}_{i_1j_1}\tau_1} \qquad (4)
\end{aligned}$$

Similarly, one obtains,

$$\begin{aligned}
&\langle B^\dagger_{ijR}(t)B_{i'j'L}(\tau)B^\dagger_{i_1j_1L}(\tau_1)B^\dagger_{i_2j_2L}(\tau_2)B_{i_3j_3R}(\tau_3)B_{i_4j_4R}(\tau_4)\rangle = \delta_{jj'}\delta_{i'i_1}\delta_{ii_3}\delta_{j_3i_4}\delta_{j_4g}\delta_{i_2j_2}\delta_{j_2g} \\
&e^{-i\mathcal{E}_{i_4g}\tau_4}e^{-i\mathcal{E}_{i_3j_3}\tau_3}e^{i\mathcal{E}_{ij}t}e^{-i\mathcal{E}_{i'j'}\tau}e^{i\mathcal{E}_{i_1j_1}\tau_1}e^{i\mathcal{E}_{i_2g}\tau_2} \\
&\langle B^\dagger_{ijR}(t)B_{i'j'L}(\tau)B^\dagger_{i_1j_1L}(\tau_1)B_{i_2j_2L}(\tau_2)B^\dagger_{i_3j_3L}(\tau_3)B_{i_4j_4R}(\tau_4)\rangle = \delta_{jj'}\delta_{i'i_1}\delta_{ii_4}\delta_{j_1j_2}\delta_{j_4g}\delta_{i_2i_3}\delta_{j_3g} \\
&e^{-i\mathcal{E}_{i_4g}\tau_4}e^{i\mathcal{E}_{ij}t}e^{-i\mathcal{E}_{i'j'}\tau}e^{i\mathcal{E}_{i_1j_1}\tau_1}e^{-i\mathcal{E}_{i_2j_2}\tau_2}e^{i\mathcal{E}_{i_3g}\tau_3} \\
&\langle B^\dagger_{ijR}(t)B_{i'j'L}(\tau)B^\dagger_{i_1j_1L}(\tau_1)B_{i_2j_2L}(\tau_2)B^\dagger_{i_3j_3L}(\tau_3)B_{i_4j_4R}(\tau_4)\rangle = \delta_{jj'}\delta_{i'i_1}\delta_{ii_4}\delta_{j_1j_2}\delta_{j_4g}\delta_{i_2i_3}\delta_{j_3g} \\
&e^{-i\mathcal{E}_{i_4g}\tau_4}e^{i\mathcal{E}_{ij}t}e^{-i\mathcal{E}_{i'j'}\tau}e^{i\mathcal{E}_{i_1j_1}\tau_1}e^{-i\mathcal{E}_{i_2j_2}\tau_2}e^{i\mathcal{E}_{i_3g}\tau_3} \\
&\langle B^\dagger_{ijR}(t)B_{i'j'L}(\tau)B^\dagger_{i_1j_1L}(\tau_1)B_{i_2j_2R}(\tau_2)B^\dagger_{i_3j_3R}(\tau_3)B_{i_4j_4R}(\tau_4)\rangle = \delta_{jj'}\delta_{i_2i}\delta_{i_1i'}\delta_{j_2j_3}\delta_{i_4i_3}\delta_{j_4g}\delta_{j_1g} \\
&e^{-i\mathcal{E}_{i_4g}\tau_4}e^{i\mathcal{E}_{i_3j_3}\tau_3}e^{-i\mathcal{E}_{i_2j_2}\tau_2}e^{i\mathcal{E}_{ij}t}e^{-i\mathcal{E}_{i'j'}\tau}e^{i\mathcal{E}_{i_1g}\tau_1} \qquad (5)
\end{aligned}$$

where the subscripts i_1, i_2, etc., denote molecular states, $|g\rangle, |e\rangle, |e'\rangle, ..., |f\rangle$ with energies $\mathcal{E}_g, \mathcal{E}_e, \mathcal{E}'_e, ..., \mathcal{E}_f$, respectively..

By substituting Eq. (5) in Eq. (3) in the main text and then in Eq. (1) in the main text, the signal can be recast as $R(\omega_s) = \sum_{n=1,6} \mathrm{Re}\ R^{(n)}(\omega_s)$, with

$$R^{(1)}(\omega_s) = \frac{4}{\hbar^2}\sum_{\{\lambda\}}\mathcal{M}^{ij;ij;ig;ig}_{\lambda\lambda\lambda_1\lambda_2}\int\frac{d\omega_1}{2\pi}\frac{iD^{-+LR}_{\lambda_1\lambda_2}(\omega_1,\omega_1)}{|\omega_1-\mathcal{E}_{ig}+i\eta|^2(\omega_s-\omega_1+\mathcal{E}_{jg}-i\eta)} \qquad (6)$$

$$R^{(2)}(\omega_s) = \frac{12}{\hbar^6}\sum_{\{\lambda\}}\int \frac{d\omega_1 d\omega_2 d\omega_3}{(2\pi)^3}\frac{(-i)\mathcal{M}^{fj;fj;fe;eg;e'g;fe'}_{\lambda\lambda\lambda_1\lambda_2\lambda_3\lambda_4} D^{--++LLRR}_{\lambda_1\lambda_2\lambda_3\lambda_4}(\omega_1,\omega_2,\omega_3,\omega_1+\omega_2-\omega_3)}{(\omega_2-\mathcal{E}_{eg}+i\eta)|\omega_1+\omega_2-\mathcal{E}_{fg}+i\eta|^2(\omega_3-\mathcal{E}_{e'g}-i\eta)} \times \frac{1}{(\omega_s-\omega_1-\omega_2+\mathcal{E}_{jg}-i\eta)} + (\lambda_1 \Leftrightarrow \lambda_2) + (\lambda_3 \Leftrightarrow \lambda_4) + (\lambda_1 \Leftrightarrow \lambda_2, \lambda_3 \Leftrightarrow \lambda_4) \tag{7}$$

$$R^{(3)}(\omega_s) = \sum_{\{\lambda\}}\int \frac{d\omega_1 d\omega_2 d\omega_3}{(2\pi)^3}\frac{(24i/\hbar^6)\mathcal{M}^{ij;ij;ij';i'j';i'g;ig}_{\lambda\lambda\lambda_1\lambda_2\lambda_3\lambda_4} D^{--++LLLR}_{\lambda_1\lambda_2\lambda_3\lambda_4}(\omega_1,\omega_1-\omega_2-\omega_3,\omega_2,\omega_3)}{(\omega_2+\mathcal{E}_{i'g}-i\eta)(\omega_1-\omega_3+\mathcal{E}_{jg}-i\eta)(\omega_3-\mathcal{E}_{ij'}-\mathcal{E}_{ig}+i\eta)(\omega_3-\mathcal{E}_{ig}-i\eta)} \times \frac{1}{(\omega_3-\omega_s+\mathcal{E}_{j'g}+i\eta)} + (\lambda_1 \Leftrightarrow \lambda_3) \tag{8}$$

$$R^{(4)}(\omega_s) = \sum_{\{\lambda\}}\int \frac{d\omega_1 d\omega_2 d\omega_3}{(2\pi)^3}\frac{(24i/\hbar^6)\mathcal{M}^{e'g;e'g;eg;fe';fe;e'g}_{\lambda\lambda\lambda_1\lambda_2\lambda_3\lambda_4} D^{--++LLLR}_{\lambda_1\lambda_2\lambda_3\lambda_4}(\omega_1,\omega_1-\omega_2-\omega_3,\omega_2,\omega_3)}{(\omega_2+\mathcal{E}_{fe}-i\eta)(\omega_1-\omega_3+\mathcal{E}_{e'e}-i\eta)|\omega_3-\mathcal{E}_{e'g}+i\eta|^2(\omega_3-\omega_s+i\eta)} + (\lambda_1 \Leftrightarrow \lambda_3) \tag{9}$$

$$R^{(5)}(\omega_s) = \sum_{\{\lambda\}}\int \frac{d\omega_1 d\omega_2 d\omega_3}{(2\pi)^3}\frac{(24i/\hbar^6)\mathcal{M}^{ij;ij;ig;ij';i'j';i'g}_{\lambda\lambda\lambda_1\lambda_2\lambda_3\lambda_4} D^{--++LRRR}_{\lambda_1\lambda_2\lambda_3\lambda_4}(\omega_1,\omega_2,\omega_1+\omega_2-\omega_3,\omega_3)}{(\omega_3-\mathcal{E}_{i'g}-i\eta)(\omega_1+\omega_2-\mathcal{E}_{j'g}-i\eta)|\omega_1-\mathcal{E}_{ig}+i\eta|^2} \times \frac{1}{(\omega_1+\omega_s-\mathcal{E}_{ij}-\mathcal{E}_{ig}+i\eta)} + (\lambda_2 \Leftrightarrow \lambda_4) \tag{10}$$

$$R^{(6)}(\omega_s) = \sum_{\{\lambda\}}\int \frac{d\omega_1 d\omega_2 d\omega_3}{(2\pi)^3}\frac{(24i/\hbar^6)\mathcal{M}^{e'g;e'g;e'g;fe;fe';eg}_{\lambda\lambda\lambda_1\lambda_2\lambda_3\lambda_4} D^{--++LRRR}_{\lambda_1\lambda_2\lambda_3\lambda_4}(\omega_1,\omega_2,\omega_1+\omega_2-\omega_3,\omega_3)}{(\omega_3-\mathcal{E}_{eg}-i\eta)(\omega_1-\omega_3-\mathcal{E}_{fg}-i\eta)|\omega_1-\mathcal{E}_{e'g}-i\eta|^2(\omega_1-\omega_s+i\eta)} + (\lambda_2 \Leftrightarrow \lambda_4) \tag{11}$$

where the sum over the repeated indices i, j, i', j' runs over all excited states of the molecule while sums over e, e' are restricted to the singly excited states, and $\{\lambda\}$ denotes a summation over all possible values of the polarizations for $\lambda, \lambda_i, i = 1, 2, 3, 4$. Note that $\mathcal{M}^{ij;ij;ig;ig}_{\lambda\lambda\lambda_1\lambda_2} = (\mu_{ij}\cdot\epsilon_\lambda)(\mu^*_{ij}\cdot\epsilon_\lambda)(\mu_{ig}\cdot\epsilon_{\lambda_1})(\mu^*_{ig}\cdot\epsilon_{\lambda_2})$ and $\mathcal{M}^{fj;fj;fe;eg;e'g;fe'}_{\lambda\lambda\lambda_1\lambda_2\lambda_3\lambda_4} = (\mu_{fj}\cdot\epsilon_\lambda)(\mu^*_{fj}\cdot\epsilon_\lambda)(\mu_{fe}\cdot\epsilon_{\lambda_1})(\mu^*_{eg}\cdot\epsilon_{\lambda_2})(\mu_{e'g}\cdot\epsilon_{\lambda_3})(\mu^*_{fe'}\cdot\epsilon_{\lambda_4})$, etc. The six terms in Eqs. (6) -(11) correspond to the six diagrams given in Fig. 1 in the main text.

Nonperturbative calculation of the entangled-field correlation functions

Entangled ("signal-idler") photon pairs are created by the interaction of the pump field with a nonlinear PDC crystal. The entangled-field output is fully characterized by various correlations of the field operators, known as one-particle propagators that are encoded in the effective action S_{eff} of the field. The entangled-photon state is determined by the amplitude E of the pump-field and by the nonlinear (second-order $\chi^{(2)}$) response of the PDC crystal of length l along the z-axis. Extension of the crystal in the $x-$ and $y-$ directions is assumed to be infinite with respect to the wavelengths of the photons involved in the process. The effective action approach leads to the following effective Hamiltonian H_{eff} for the entangled-field generation.

$$\begin{aligned} H_{eff}(z) &= \sum_{\alpha} \int \frac{d\omega}{2\pi} \left(\kappa_{i\alpha}(\omega) E^{\dagger}_{i\alpha}(\omega) E_{i\alpha}(\omega) + \kappa_{s\alpha}(\omega) E^{\dagger}_{s\alpha}(\omega) E_{s\alpha}(\omega) \right) \\ &+ \hbar \sum_{\alpha,\beta} \int \frac{d\omega d\omega'}{(2\pi)^2} \chi^{(2)}(\omega,\omega') \mathcal{E}(\omega+\omega',z) E^{\dagger}_{i\alpha}(\omega) E^{\dagger}_{s\beta}(\omega') + h.c. \end{aligned} \tag{12}$$

where $E^{\dagger}_{i\alpha}(\omega)$ is the creation operator in the "idler" mode with polarization $\epsilon_{\alpha}, \alpha$ (horizontal "H" or vertical "V"), frequency ω, $\kappa_{i\alpha}(\omega)$ is the corresponding dispersion of the mode, $\mathcal{E}(\omega, z)$ is the amplitude of the pump field at the position z along the propagation direction inside the crystal, and $\chi^{(2)}(\omega,\omega') \approx \frac{1}{2l}\sqrt{\frac{\omega_i \omega_s}{n_i^2 n_s^2}} \chi^{(2)}_{eff}(\omega,\omega')$, where l is the length of the PDC crystal along the z-axis, $\omega_{i/s}(n_{i/s})$ is the central frequency (refractive index) of the idler/signal mode, and $\chi^{(2)}_{eff}$ is the is the second-order susceptibility of the PDC crystal. The polarization ϵ_{β} is perpendicular to ϵ_{α}, $\epsilon_{\alpha} \cdot \epsilon_{\beta} = 0$. The second term in the above Hamiltonian, therefore, generates a Bell polarization state for the signal and the idler modes.

The evolution of modes inside the crystal is determined by the Heisenberg equations,

$$\frac{\partial}{\partial z} E_{i\alpha}(\omega, z) = -\frac{i}{\hbar} \kappa_{i\alpha}(\omega) E_{i\alpha}(\omega, z) - \frac{i}{\hbar} \int \frac{d\omega'}{2\pi} \chi^{(2)}(\omega,\omega') \mathcal{E}(\omega+\omega') E^{\dagger}_{s\beta}(\omega, z) \tag{13}$$

with the initial condition $E_{i\alpha}(\omega,-l)$ defined at $z=-l$. $E_{s\alpha}$ is obtained by interchanging the indices i and s in Eq. (13).

The formal solution of Eq. (13) is

$$E_{i\alpha}(\omega,0)=U_{ii}^{\alpha\alpha}(\omega,\omega')E_{i\alpha}(\omega',-l)+V_{is}^{\alpha\beta}(\omega,\omega')E_{s\beta}^{\dagger}(\omega',-l) \tag{14}$$

where β denotes a polarization ϵ_β perpendicular to ϵ_α. The entangled field propagators may be recast in terms of the functions $U(\omega,\omega')$ and $V(\omega,\omega')$ introduced in Eq. (14). For example, $D_{si;\alpha\alpha'}^{--LL}(\omega,\omega')\equiv\mathcal{D}_{si;\alpha\alpha'}^{--}(\omega,\omega')=\langle E_{s\alpha}(\omega)E_{i\alpha'}(\omega')\rangle$ is given by,

$$\mathcal{D}_{si;\alpha\alpha'}^{--}(\omega,\omega') \;=\; \delta_{\alpha\beta}\int\frac{d\omega_1}{2\pi}U_{ss}^{\alpha\alpha}(\omega,\omega_1,0)V_{is}^{\alpha'\beta}(\omega',\omega_1,0), \tag{15}$$

where $U_{ss}^{\alpha\alpha}(\omega,\omega',z)$ and $V_{is}^{\alpha\beta}(\omega,\omega',z)$ are the solutions of the coupled equations for $\tilde{U}_{ss}^{\alpha\alpha}(\omega,\omega',z)=e^{i\kappa_{s\alpha}(\omega)z}U_{ss}^{\alpha\alpha}(\omega,\omega',z)$ and $\tilde{V}_{is}^{\alpha\beta}(\omega,\omega',z)=e^{i\kappa_{i\alpha}(\omega)z}V_{is}^{\alpha\beta}(\omega,\omega',z)$,

$$\begin{aligned}
\frac{\partial}{\partial z}\tilde{U}_{ss}^{\alpha\alpha}(\omega,\omega',z) &= -i\int\frac{d\omega_1}{2\pi}\chi^{(2)}(\omega,\omega_1)\mathcal{E}(\omega+\omega_1)e^{-i\Delta k_{si}^{\alpha\beta}(\omega,\omega_1)z}[\tilde{V}_{is}^{\beta\alpha}(\omega_1,\omega',z)]^*\\
\frac{\partial}{\partial z}\tilde{V}_{is}^{\alpha\beta}(\omega,\omega',z) &= -i\int\frac{d\omega_1}{2\pi}\chi^{(2)}(\omega,\omega_1)\mathcal{E}(\omega+\omega_1)e^{-i\Delta k_{is}^{\alpha\beta}(\omega,\omega_1)z}[\tilde{U}_{ss}^{\beta\beta}(\omega_1,\omega',z)]^*
\end{aligned} \tag{16}$$

with $\Delta k_{is}^{\alpha\beta}(\omega,\omega')=k_p(\omega+\omega')-\kappa_{i\alpha}(\omega)-\kappa_{s\beta}(\omega')$ and $k_p(\omega+\omega')$ being the momentum of the pump-pulse at frequency $\omega+\omega'$. $\mathcal{D}_{si\alpha\alpha'}^{++}(\omega,\omega')$ is obtained from (15) by replacing the field annihilation operators by the corresponding creation operators.

Note that $U^{\alpha\alpha'}$ is diagonal in the polarization indices α,α' while $V^{\alpha\beta}$ is off-diagonal. This, together with Eq. (15), implies that the propagators $\mathcal{D}_{si\alpha\alpha'}^{++}$ and $\mathcal{D}_{si\alpha\alpha'}^{--}$ are non-zero only for orthogonal polarizations ϵ_α and $\epsilon_{\alpha'}$. Similarly, $\mathcal{D}_{ss\alpha\alpha'}^{-+}$ and $\mathcal{D}_{ii\alpha\alpha'}^{-+}$ survive iff the α and α' polarizations are parallel. Finally, Eqs. (16) can be computed numerically for an arbitrary pump spectral envelop $\mathcal{E}(\omega)$, crystal response function $\chi^{(2)}(\omega)$, and dispersions of the pump, idler and signal modes.

Below we derive analytic expressions for a narrow pump $\mathcal{E}(\omega)=2\pi E_p\delta(\omega_p-\omega)$ with

frequency ω_p. The main simplification in this case comes from the fact that the z-dependent coefficients in the differential equation (16) drops out and the evolution inside the crystal does not require z-ordering. The ω_1 integration in Eq. (16) can be performed trivially and we finally obtain, $U_{ss}^{\alpha\alpha}(\omega,\omega',0) = \delta(\omega-\omega')\mathcal{U}_{ss}^{\alpha\alpha}(\omega,\bar{\omega})$ and $V_{is}^{\alpha\beta}(\omega,\omega',0) = \delta(\omega+\omega'-\omega_p)\mathcal{V}_{is}^{\alpha\beta}(\omega,\bar{\omega})$ where $\bar{\omega} = \omega_p - \omega$ and,

$$\mathcal{U}_{ss}^{\alpha\alpha}(\omega,\bar{\omega}) = e^{-i\frac{l}{2}\bar{\kappa}_{si}^{\alpha\beta}(\omega,\bar{\omega})}\left[\cosh\left(\frac{\kappa_{si}^{\alpha\beta}(\omega,\bar{\omega})l}{2}\right) + i\frac{\Delta k_{si}^{\alpha\beta}(\omega,\bar{\omega})}{\kappa_{si}^{\alpha\beta}(\omega,\bar{\omega})}\sinh\left(\frac{\kappa_{si}^{\alpha\beta}(\omega,\bar{\omega})l}{2}\right)\right] \quad (17)$$

$$\mathcal{V}_{is}^{\alpha\beta}(\omega,\bar{\omega}) = -2i\frac{E_p\chi^{(2)}(\omega,\bar{\omega})}{\kappa_{is}^{\alpha\beta}(\omega,\bar{\omega})}e^{\frac{i}{2}\bar{\kappa}_{si}^{\beta\alpha}(\bar{\omega},\omega)l}\sinh\left(\frac{\kappa_{is}^{\alpha\beta}(\omega,\bar{\omega})l}{2}\right) \quad (18)$$

where $\bar{\kappa}_{si}^{\alpha\beta}(\omega,\omega') = k_p(\omega_p) + \kappa_{s\alpha}(\omega) - \kappa_{i\beta}(\omega')$, and

$$\kappa_{si}^{\alpha\beta}(\omega,\omega') = \sqrt{4|E_p|^2\chi^{(2)}(\omega,\omega')\chi^{(2)}(\omega',\omega) - (\Delta k_{si}^{\alpha\beta}(\omega,\omega'))^2}.$$

$U_{ii}^{ss}(\omega,\omega',0)$ and $V_{si}^{\alpha\beta}(\omega,\omega',0)$ are obtained from Eqs. (17) and (18), respectively, by interchanging $i \Leftrightarrow s$.

Extension to a narrow pump pulse: The above results obtained for a CW-pump can be extended approximately for a sufficiently narrow pump pulse by using the Wigner transformation of the pulse. Assuming that the pump amplitude varies slowly enough so that the phase, which varies with frequency ω_p, is fast enough compared to the time-scale of the envelop (determined by the band-width), we extend the CW-pulse results as follows. First we re-write $U_{ss}^{\alpha\alpha}(\omega,\omega',0) = \int dt e^{i(\omega-\omega')t}\mathcal{U}_{ss}^{\alpha\alpha}(\omega,\omega_p-\omega')$ and $V_{is}^{\alpha\beta}(\omega,\omega',0) = \int dt e^{i(\omega+\omega'-\omega_p)t}\mathcal{V}_{is}^{\alpha\beta}(\omega,\omega_p-\omega')$. This is exact for a CW-pump for any pump amplitude, E_p. We assume that the pump amplitude E_p varies slowly enough so that E_p can be replaced by its values at different times, which makes the functions $\mathcal{U}$ and $|calV$ time dependent. Thus

for a narrow but finite bandwidth pump we can use,

$$U_{ss}^{\alpha\alpha}(\omega,\omega',0) = \int dt\ e^{i(\omega-\omega')t}\ \mathcal{U}_{ss}^{\alpha\alpha}(\omega,\omega_p-\omega',t)$$

$$V_{is}^{\alpha\beta}(\omega,\omega',0) = \int\ dt\ e^{i(\omega+\omega'-\omega_p)t}\ \mathcal{V}_{is}^{\alpha\beta}(\omega,\omega_p-\omega',t).$$

These equations are used to evaluate the correlation functions for a narrow pump bandwidths in the main text.

The Two-Photon Correlation Function (TPCF) for a finite-bandwidth pump

The TPCF $D_{si,HV}^{--}(\omega,\omega_1)$ in Eq. 15 is evaluated numerically by solving Eqs. (16) using,

$$\begin{aligned}\Delta k_{si}^{HV}(\omega,\omega_1) &= \frac{\omega-\bar{\omega}_s}{v_{1,H}} + \frac{\omega_1-\bar{\omega}_i}{v_{2,V}}\\ \Delta k_{is}^{VH}(\omega,\omega_1) &= \frac{\omega-\bar{\omega}_i}{v_{2,V}} + \frac{\omega_1-\bar{\omega}_s}{v_{1,H}}\end{aligned} \tag{19}$$

where v_1=$v_p - v_{a,X}$, and $v_2 = v_p - v_{i,X}$ with v_p, $v_{s,X}$, and $v_{i,X}$ being group velocities of the pump, the signal, and the idler photons, respectively, with polarization ϵ_X, and $\bar{\omega}_s$ ($\bar{\omega}_i$) represents the center frequency of the signal (idler) photon. We take $l = 20\,\mu$m crystal length, and the following spectral envelope of the pump field.

$$\mathcal{E}(\omega) = \frac{E_p}{\sqrt{2\pi\sigma_p^2}} e^{-(\omega_p-\omega)^2/(2\sigma_p^2)} \tag{20}$$

where E_p, $\bar{\omega_p}$, and σ_p represent the amplitude, central frequency, and the spectral width of the field, respectively.

The pump-intensity associated with Eq. 20 can be obtained using the following expres-

sion,

$$I_p = \frac{1}{2} c\epsilon_0 n_p |E_p|^2 \tag{21}$$

where E_p is the pump-pulse amplitude, and n_p is the refractive index of the PDC crystal for the pump-pulse, c is the speed of light, and ϵ_0 is the permittivity of free space.

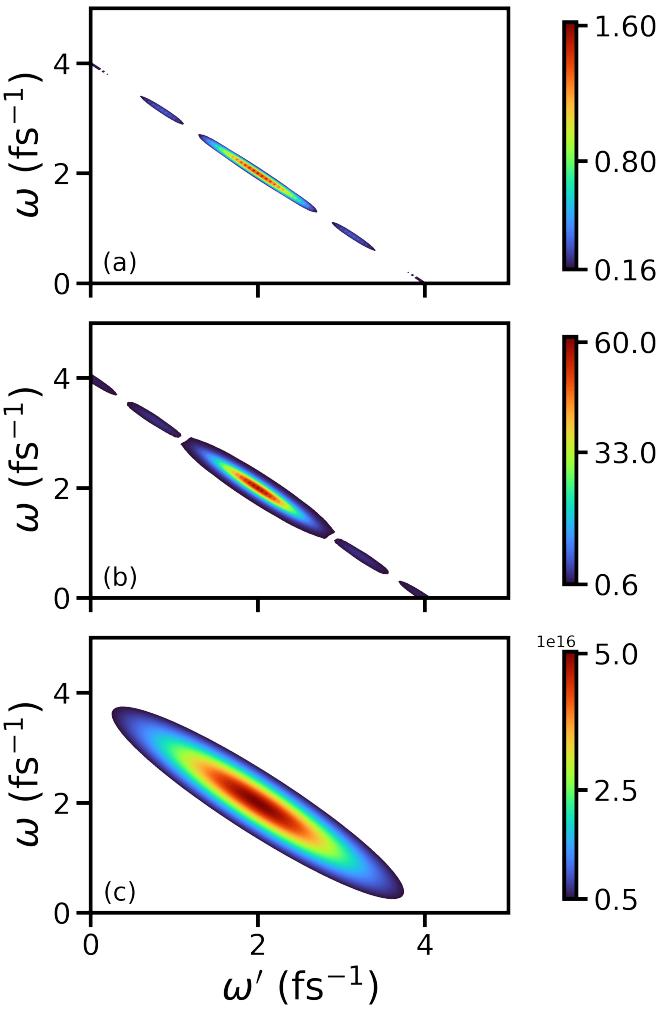

Figure S1: 2D frequency-dispersed plots for $D^{--}_{si,HV}$ (Eq. 14) with σ_p=0.1 fs^{-1} and (a) I_p=5.9×10^5 W/cm^2, (b) I_p=5.9×10^7 W/cm^2, and (c) I_p=1.47×10^9 W/cm^2 are shown. Other parameters: $v_{1,H}$=$v_{2,H}$=10 μm·fs^{-1}, $v_{1,V}$=$v_{2,V}$=-10 μm·fs^{-1} $\bar{\omega_p}$=4 fs^{-1}, and $\bar{\omega_s}$=2 fs^{-1}.

Figure S1 displays 2D frequency-dispersed plots for $D^{--}_{si,HV}$ for a fixed pump bandwidth of σ_p=0.1 fs^{-1} and different pump intensities. Figure S1(a) is constructed using the weakest pump with I_p=5.9×10^5 W/cm^2. Frequencies are clearly anti-correlated. For increased

amplitude I_p=5.9×10^7 W/cm^2 the signal strength increases, but the anti-correlation is still intact, as shown in Fig. S1(b). Further increase to I_p=1.47×10^9 W/cm^2 leads to vanishing of the features visible in the earlier two cases, as evident in Fig. S1(c). However, the frequency anti-correlation is still present in the signal. The amplitude of the correlation function increases exponentially with the pump amplitude. To study the impact of the pump-width on

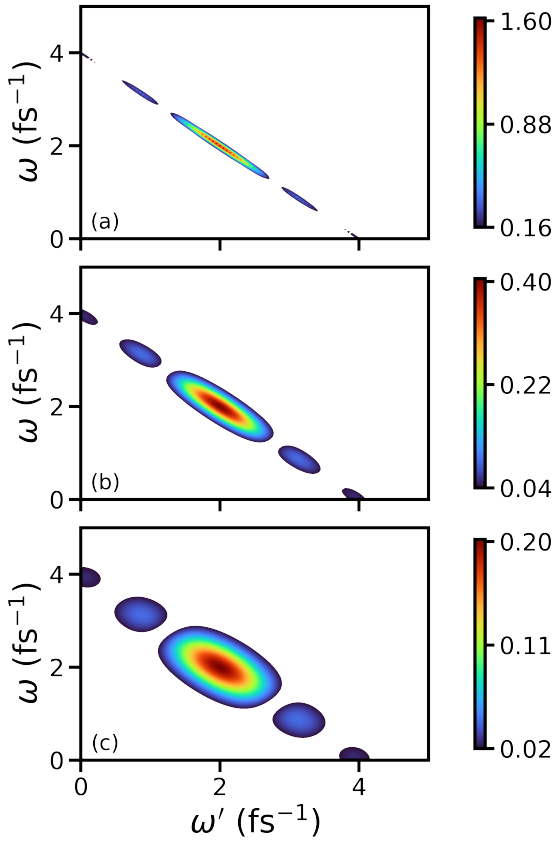

Figure S2: 2D frequency-dispersed plots for $D^{--}_{si,HV}$ (see Eq. 14) for I_p=5.9×10^5 W/cm^2 with (a) σ_p=0.1 fs^{-1}, (b) σ_p=0.5 fs^{-1}, and (c) σ_p=1.0 fs^{-1} are shown. Other system parameters: $v_{1,H}$=$v_{2,H}$=10 μm·fs^{-1}, $v_{1,V}$=$v_{2,V}$=-10 μm·fs^{-1} $\bar{\omega_p}$=4 fs^{-1}, and $\bar{\omega_s}$=2 fs^{-1}.

the frequency anti-correlation, we present in Fig. S2 frequency dispersed plots of $D^{--}_{si,HV}$ for a fixed pump amplitude but different band-widths. For a narrowband pump with σ_p=0.1 fs^{-1}, a strong frequency anti-correlation is present, as shown in Fig. S2(a). However, for a larger pulse width with σ_p=0.5 fs^{-1}, the signal spreads along the diagonal, resulting in a decrease in the frequency anti-correlation, as shown in Fig. S2(b). A similar trend is seen in Fig. S2(c),

and the frequency anti-correlation continues to decrease. Note that the absolute strength of the field correlation function falls with an increase in the pump bandwidth as well.

$g^{(2)}(\tau)$ with zero bandwidth pump pulse

For a zero-band-width pump, Eqs. (17) and (18) can be solved for the dynamical Eq. (16). $D^{--}_{si\alpha\alpha'}(\omega,\omega')$ in Eq. (15) may be then expressed as (we remove polarization indices assuming that the "idler" and "signal" modes have fixed orthogonal polarizations),

$$\begin{aligned} D^{--}_{si}(\omega,\omega') &= -\frac{2i}{h}\delta(\omega+\omega'-\omega_p)\frac{\chi^{(2)}E_p}{\kappa_{is}(\omega\bar{\omega})}e^{-i\frac{l}{2}(\bar{\kappa}_{si}(\omega,\bar{\omega})-\bar{\kappa}_{si}(\bar{\omega},\omega))}\sinh\left(\frac{l}{2}\kappa_{is}(\bar{\omega},\omega)\right) \\ &\times \left(\cosh\left(\frac{l}{2}\kappa_{si}(\omega,\bar{\omega})\right)+i\frac{\Delta k_{si}(\omega,\bar{\omega})}{\kappa_{si}(\omega,\bar{\omega})}\sinh\left(\frac{l}{2}\kappa_{si}(\omega,\bar{\omega})\right)\right) \end{aligned} \tag{22}$$

where $\bar{\omega}=\omega_p-\omega$ and the phase miss-match $\Delta k_{si}(\omega,\bar{\omega})$ is approximated using Taylor expansion $\kappa_{s\alpha}(\omega)\sim\kappa_{s\alpha}(\omega_s)+(\omega-\omega_s)T_{s\alpha}/l$ and $\kappa_{i\alpha}(\omega')\sim\kappa_{i\alpha}(\omega_i)+(\omega-\omega_i)T_{i\alpha}/l$ around the central frequencies ω_i and ω_s of the "idler" and "signal" photons, respectively, to obtain, $\Delta k_{si}(\omega,\bar{\omega})\approx-\frac{\Delta T}{l}(\omega-\omega_s)$ and $\Delta k_{is}(\omega,\bar{\omega})\approx\frac{\Delta T}{l}(\omega-\omega_i)$ with $\Delta T=T_s-T_i$ being the entanglement time. Similarly, for the intra-mode correlations, we get

$$D^{+-}_{ii}(\omega,\omega') = 4\delta(\omega-\omega')\left|\frac{E_p\chi^{(2)}}{\kappa_{si}(\omega,\bar{\omega})}\sinh\left(\frac{\kappa_{si}(\omega,\bar{\omega})}{2}l\right)\right|^2. \tag{23}$$

Note that for the narrow band-width pump, all intra-mode (inter-mode) propagators are diagonal (anti-diagonal) in the frequency space. This allows us to simplify the expression for $g^{(2)}(\tau)$ using Eq. (**??**).

$$\begin{aligned} g^{(2)}(\tau) &= 1+\frac{1}{S(\tau)}\int\frac{d\omega d\omega'}{(2\pi)^2}\sum_{qq'=i,s}D^{+-}_{qq}(\omega,\omega)D^{+-}_{q'q'}(\omega',\omega')e^{-i(\omega-\omega')\tau} \\ &+ \sum_{q\neq q'}\sum_{q_1\neq q'_1}\frac{1}{S(\tau)}\int\frac{d\omega d\omega'}{(2\pi)^2}D^{++}_{qq'}(\omega,\omega)D^{--}_{q_1q'_1}(\omega',\omega')e^{i(\omega_p-\omega-\omega')\tau}. \end{aligned} \tag{24}$$

For simplicity, we assume a degenerate PDC process $\omega_i=\omega_s$. In this case, $g^{(2)}(\tau)$

simplifies to,

$$
\begin{aligned}
g^{(2)}(\tau) &= 1+\frac{1}{S(\tau)}\left(\frac{8(\chi E_p l)^2}{\Delta T}\right)^2\left|\int\frac{d\omega}{2\pi}\frac{\sinh^2(\frac{1}{2}\sqrt{(2\chi E_p l)^2-\omega^2})}{(2\chi E_p l)^2-\omega^2}e^{i\omega\frac{\tau}{\Delta T}}\right|^2 \\
&+ \frac{1}{S(\tau)}\left(\frac{2\chi E_p l}{\Delta T}\right)^2\left|\int\frac{d\omega}{2\pi}\frac{\sinh(\sqrt{(2\chi E_p l)^2-\omega^2})}{\sqrt{(2\chi E_p l)^2-\omega^2}}e^{i\omega\frac{\tau}{\Delta T}}\right|^2 \\
&\approx 1+\frac{1}{\pi S(\tau)}\left(\frac{(\sinh(\chi E_p l))^2}{\alpha_1\Delta T}\right)^2 e^{-\frac{1}{2}\left(\frac{\tau}{\alpha_1\Delta T}\right)^2}+\frac{1}{2\pi S(\tau)}\left(\frac{\sinh(2\chi E_p l)}{\alpha_2\Delta T}\right)^2 e^{-\frac{(\tau+\tau_0)^2+(\tau-\tau_0)^2}{(\alpha_2\Delta T)^2}} \quad (25)
\end{aligned}
$$

where in the second line we have used the approximation of steepest descent method to evaluate the integral, $\alpha_n = \sqrt{n\chi E_p l\ coth(n\chi E_p l)-1}/(2\chi E_p l), n = 1, 2$, and $\tau_0 = T_i + T_s$. The normalization $S(\tau) = \mathcal{S}^2$ is independent of delay with $\mathcal{S} = 2\int\frac{d\omega}{2\pi}|V_{si}(\omega,\omega)|^2$, which gives, $\mathcal{S} = \frac{(\sinh(\chi E_p l))^2}{\sqrt{\pi}\alpha_1|\Delta T|}$. Substituting this in the above equation for $g^{(2)}(\tau)$, we get

$$
g^{(2)}(\tau) = 1+e^{-\frac{1}{2}\left(\frac{\tau}{\alpha_1\Delta T}\right)^2}+2\left(\frac{\alpha_1}{\alpha_2}\coth(\chi E_p l)\right)^2 e^{-\frac{(\tau+\tau_0)^2+(\tau-\tau_0)^2}{(\alpha_2\Delta T)^2}}. \quad (26)
$$

The intra-mode contribution decays to unity while the inter-mode contribution decays to zero at large τ. For $\tau = 0$, the intra-mode part is independent on the pump intensity and is equal to 2, while the inter-mode contribution decays rapidly with increasing pump intensity for small values of pump intensities, $E_p < 1/(\chi l)$, and saturates to unity for large pump intensities.